Research Article

Lanthanum sulfide/graphene oxide composite thin films and their supercapacitor application

Trupti T. Ghogare[1] · Abhishek C. Lokhande[2] · Rahul B. Pujari[1] · Chandrakant D. Lokhande[1]

Abstract

In this study, graphene oxide, lanthanum sulfide and their composite thin films are prepared using simple and inexpensive chemical methods and their supercapacitive performance is evaluated. The X-ray diffraction study shows the formation of mixed-phase lanthanum sulfide with monoclinic α-LaS$_2$ and tetragonal La$_5$S$_7$. Field emission scanning electron microscopy images show porous surface morphology of lanthanum sulfide and composite thin films. The supercapacitive performance of composite film tested in 1 M Na$_2$SO$_4$ electrolyte shows highest specific capacitance of 312 F g^{-1} at a 5 mV s^{-1} scan rate.

Keywords Graphene oxide · Lanthanum sulfide · Successive ionic layer adsorption reaction · Supercapacitor · Thin films

1 Introduction

Electrochemical energy storage is a high requirement for intermittent renewable energy sources. The energy storage devices mainly include lithium-ion batteries and supercapacitors [1, 2]. The energy storage in the supercapacitor is established by two mechanisms. One is the electrical double-layer capacitive (EDLC) and another one is the pseudocapacitive. Electrical double-layer capacitors (EDLC) based on quick ion adsorption/desorption and pseudocapacitors originated from fast faradaic charge transfer reactions occurred at electrode surface [3, 4]. Earlier used pseudocapacitive materials were transition metal oxides and conducting polymers having both the improved energy and power densities [5, 6].

Lanthanum sulfide is one of the promising rare earth materials used recently as supercapacitor electrode. The films of lanthanum sulfide with phase of α-La$_2$S$_3$ are prepared using successive ionic layer adsorption and reaction (SILAR) method by Patil et al. [7] who showed maximum capacitance of 256 F g^{-1}. Patil et al. [8] studied the effect of aqueous electrolyte on the performance of La$_2$S$_3$ films. Also, Ghogare et al. [9] prepared β-LaS$_2$ film by hydrothermal method and reported a specific capacitance of 121.42 F g^{-1}. Lanthanum sulfide electrode showed good energy storage capacity in both aqueous and non-aqueous electrolytes [10].

Graphene oxide (GO) is more motivating because of its monolayer arrangement of carbon atoms in a honeycomb network with SP^2 bonding configuration [11]. The GO-based materials provide high surface area backbone metal oxides/sulfides that increase capacitance of GO-based composite electrode through faradaic reactions [12]. The GO is one of the most important derivatives of graphene, which is characterized by a layered structure with oxygen functional group attached on the basal planes and edges because of which GO has the hydrophilic nature, so that water dispersion of GO provides an easy path for preparing its composite with metal sulfides [13, 14].

This article reports for the first time the preparation of lanthanum sulfide/GO composite thin films prepared by successive ionic layer adsorption and reaction method

✉ Chandrakant D. Lokhande, l_chandrakant@yahoo.com | [1]Centre for Interdisciplinary Research, D.Y. Patil Education Society (Deemed to be University), Kolhapur 416 006, India. [2]Department of Material Science and Engineering, Chonnam National University, Gwangju 500 757, South Korea.

on a stainless steel substrate. The GO is deposited using layer-by-layer (LBL) deposition method. For a preparation of composite film, lanthanum sulfide electrode is deposited onto GO. The structural and morphological analyses of these films are carried out using XRD and FE-SEM techniques. Further, the electrodes are studied for supercapacitive application in 1 M Na_2SO_4 electrolyte.

2 Experimental

2.1 Synthesis of GO thin films

The GO was synthesized from graphite flakes by a modified Hummers method [15, 16]. Typically, graphite (5 g) and $NaNO_3$ (2.5 g) were mixed with 120 ml of H_2SO_4 (95%) in a 500-ml flask. The mixture was stirred for 30 min in an ice-water bath. While maintaining vigorous stirring, potassium permanganate (15 g) was added to the suspension slowly to keep the reaction temperature below 20 °C. Upon completion of potassium permanganate addition, the ice-water bath was removed, and the mixture was kept stirring at room temperature for overnight. As the reaction proceeded, the mixture gradually became pasty, and the color turned into light brownish. After overnight stirring, 150 ml double-distilled water (DDW) was slowly added to the paste with vigorous agitation while the paste color changed to yellow. The diluted suspension was stirred for another 15 min, and 50 ml 30% H_2O_2 was added to the mixture. For purification, the mixture was washed with DDW for several times until pH 7 is achieved. After filtration, brownish-colored GO was obtained.

For the preparation of GO thin films, layer-by-layer (LBL) method was used. The prepared GO of 1 mg ml^{-1} was exfoliated in 120 ml DDW using ultrasonic treatment for 1 h. This process provided a well-dispersed brown-colored solution of GO sheets. A 40-ml GO from this solution was taken and the cleaned glass and stainless steel substrate were immersed and kept for 40 s, then withdrawn gradually and dried with air drier for 20 s, to improve the adherence of GO sheets to the substrate. Such 100 cycles were repeated to achieve the optimum thickness of GO films.

2.2 Synthesis of lanthanum sulfide thin film

The deposition of lanthanum sulfide thin film by SILAR method comprises the successive immersion of the substrate in cationic precursor and anionic precursor solutions at room temperature. An aqueous 0.1 M $LaCl_3 \cdot 7H_2O$ solution is used as the cationic precursor, and 0.05 M Na_2S solution was utilized as the anionic precursor. The

cleaned stainless steel substrate is immersed in the cationic precursor for 20 s, and La^{+3} ions are adsorbed on the substrate, followed by 10-s rinsing in DDW to remove the loosely bound species of La^{+3}. Successively, the substrate is dipped into the anionic precursor solution for 20 s to build a layer of lanthanum sulfide. Again, the substrate is rinsed for 10 s in DDW to take out the overloaded or unreacted species. In this way, one SILAR cycle of lanthanum sulfide deposition is completed and 100 such deposition cycles are reiterated to get the terminal thickness of the film.

2.3 Synthesis of composite thin film

For the fabrication of composite thin films, the prepared GO solution is used as the source of GO sheets; cationic precursor solution is 0.1 M $LaCl_3 \cdot 7H_2O$, and 0.05 M Na_2S is an anionic precursor solution. The single layer of composite film through LBL and SILAR methods is deposited using the procedure as follows. The well-cleaned stainless steel substrate is immersed in a solution of GO for 40 s and then air-dried for 20 s for GO sheets deposition on the substrate. Then, the substrate is dipped in the cationic precursor solution for 20 s for the adsorption of lanthanum species on the GO sheets. Then, the substrate is rinsed in DDW for 10 s to remove loosely bound species of La^{+3} species. After, the substrate is immersed in the anionic precursor solution (S^{-2}) for 20 s to form a layer of lanthanum sulfide material on GO sheets. Again, the substrate is rinsed in DDW for 10 s to separate out the overload or unreacted species. Thus, one cycle of the composite deposition is completed and 100 such deposition cycles are repeated to achieve an optimum thickness of the film. The loading GO on stainless steel is 0.069 gm cm^{-2} and loading of lanthanum sulfide is 0.083 gm cm^{-2} in composite film.

2.4 Materials characterization

The crystal structure of GO, lanthanum sulfide and composite thin film was examined using a Bruker AXS D8 advance model X-ray diffractometer with primary monochromatic radiation from Cu Ka line ($\lambda = 1.54$ Å) in the 2θ range of 10–80°. The surface morphology of thin films was observed using field emission scanning electron microscope (FE-SEM, JEOL-6360, Japan). The wettability test was conducted by contact angle measurement (water as a solvent) using Rame-Hart NRL CA Goniometer. Electrochemical measurements of GO, lanthanum sulfide and

composite thin films were taken using Zive MP1 model of Wonatech company using three-electrode cell, consisting of thin films as the working electrode, platinum as a counter electrode and the saturated calomel electrode (SCE) as a reference electrode.
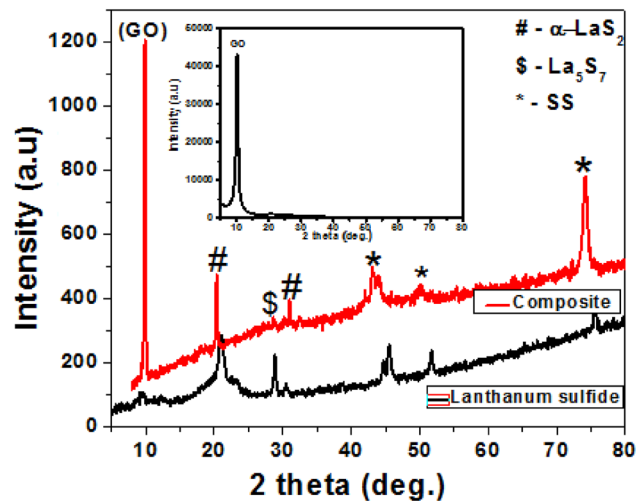

Fig. 1 X-ray diffraction patterns of **a** lanthanum sulfide, and **b** composite thin films on stainless steel substrate and inset provides XRD pattern of GO thin film
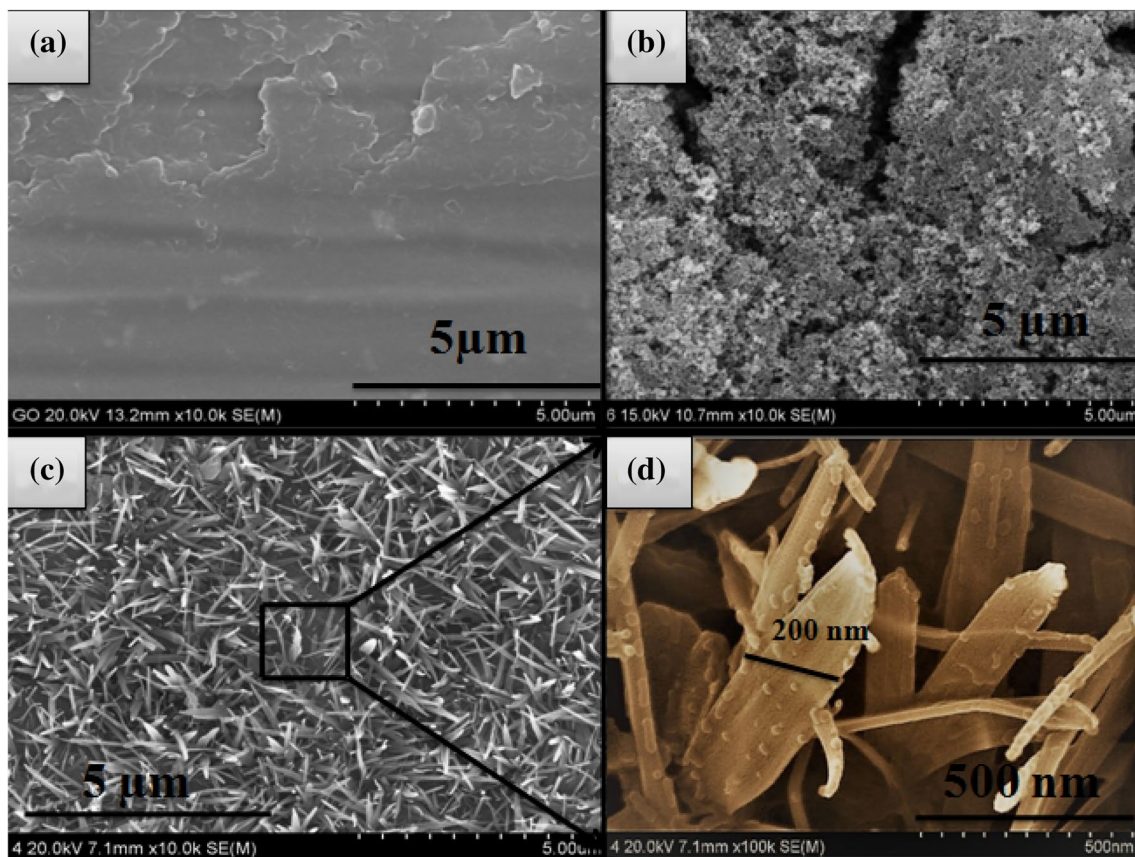
3 Results and discussion

Figure 1 shows the XRD patterns of GO, lanthanum sulfide and composite thin films on stainless steel substrate. Well-resolved diffraction peak (inset of Fig. 1) located at $2\theta = 10.1°$ indicates deposition of GO thin film. The strong peaks are marked by # at 2θ values of 20.7° and 31.1° matched with the (020) and (201) planes, respectively, of the monoclinic structure of α-LaS_2 (JCPDS No. 42-0787). A single peak is indicated by $ at $2\theta = 28.7°$ matched with the (320) plane of the tetragonal crystal structure of La_5S_7 (JCPDS No. 89-4035). The estimated size of (020) and (201) planes for lanthanum sulfide and composite thin films is found to be 1.4 and 5.4 nm, respectively.

The surface morphology of thin film plays an important role in the supercapacitive performance of material [17]. The FE-SEM micrographs of GO, lanthanum sulfide and composite thin films are shown in Fig. 2 at 10,000× magnification. It is observed from Fig. 2a that graphene

Fig. 2 FE-SEM images of **a** GO, **b** lanthanum sulfide and **c** composite thin films examined at 10,000× magnifications

oxide has homogeneous layered structure. Lanthanum sulfide (Fig. 2b) thin film shows sponge-like porous structure with grain size less than 0.5 micron. Figure 2c shows grass-like morphology for composite film consisting of thin and randomly aggregated particles grown on the GO structure. Figure 2d shows the micropetals of grass at 100 k× magnifications. The size of micropetals is typically in between 150 and 250 nm as seen at 100 kX magnification.

The angle formed between the liquid–solid interface and the liquid–vapor interface is the contact angle. The static sessile drop contact angle is measured by a contact angle goniometer using an optical subsystem to capture the profile of a pure liquid on a solid substrate. The present system includes high-resolution camera and software to capture and analyze the contact angle. The drop of the liquid applied on the solid substrate is 1 µl. For the controlling or modifying of electrode surface, wettability is an important aspect of the application of supercapacitor [18]. The water contact angle measurement photographs of films are shown in Fig. 3a–c. The GO, lanthanum sulfide and composite films show the contact angles of 66.8°, 47.6° and 37.2°, respectively. This shows that the composite film is more hydrophilic as compared with other two films which is suitable for supercapacitor application [19].

Highly porous microstructure of thin film plays an important role in supercapacitor application. The composite materials formed with Mn_3O_4 [20], NiS [21] or conducting polymer [22] with GO have demonstrated the improved capacitive performance and cycle life through the synergistic effect of both EDLC and pseudo-capacitance mechanisms [23–25]. The cyclic voltammetry measurement is taken to analyze the supercapacitive performance of GO, lanthanum sulfide and composite electrodes using three-electrode cell configuration system in 1 M Na_2SO_4 electrolyte. Figure 4a shows the comparative cyclic voltammogram (CV) curves of GO, lanthanum sulfide and composite electrodes. As the area under CV curve obtained for composite electrode is larger, the composite electrode is further studied to test its supercapacitive properties. The CV curves of composite electrodes are obtained at different scan rates. As seen from the curves in Fig. 4b, the capacitance of composite electrode decreased from 312 to 115 F g^{-1} with the increased scan rate in the range of 5–100 mV s^{-1} in the potential window of -1.0 to 0 V/SCE. The specific capacitance (Cs) of material is obtained from CV curves using the following formula:

$$Cs = \frac{1}{mv(V_{max} - V_{min})} \int_{V_{min}}^{V_{max}} I(v)dv \qquad (1)$$

where Cs is the specific capacitance in Fg^{-1}, m is the deposited mass on 1-cm^2-area substrate, v is the scan rate, $(V_{max} - V_{min})$ is the active potential applied and $I(v)$ is the current response of material.

The increment in current response with the scan rate depicts capacitive behavior. The specific capacitance (Cs) composite electrode decreases with increasing scan rate as shown in Fig. 4c. The decreased capacitance at higher scan rate is attributed to the incomplete utilization of the active electrode sites due to the limited time domain. A good cycling stability is a very important factor for supercapacitor application. The long cycling stability of composite electrode was studied in 1 M Na_2SO_4 electrolyte at 100 mV s^{-1} scan rate. Figure 4d exhibits capacitive retention of composite electrode for increasing cycles, and it shows up to 94% capacitance retention after 1000 CV cycles. Inset shows CV curves recorded at different CV cycles. During the charge/discharge process, Na$^+$ ions from the electrolyte were involved in the charge storage process of lanthanum sulfide/graphene oxide composite electrode. The reversible redox reactions by means intercalation/deintercalation of Na$^+$ ions is dependable for charge storage at composite electrode. The reaction mechanism is as follows:
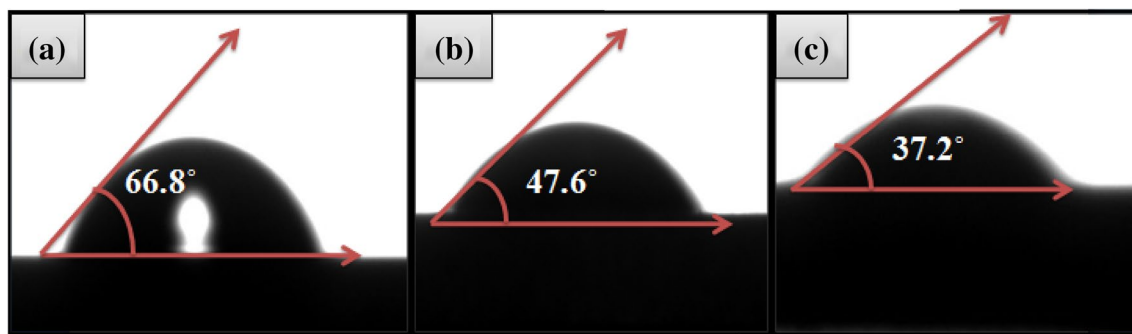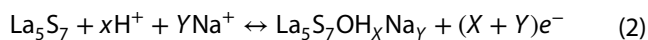
$$La_5S_7 + xH^+ + YNa^+ \leftrightarrow La_5S_7OH_XNa_Y + (X+Y)e^- \qquad (2)$$

Fig. 3 Contact angles of **a** GO, **b** lanthanum sulfide and **c** composite thin films
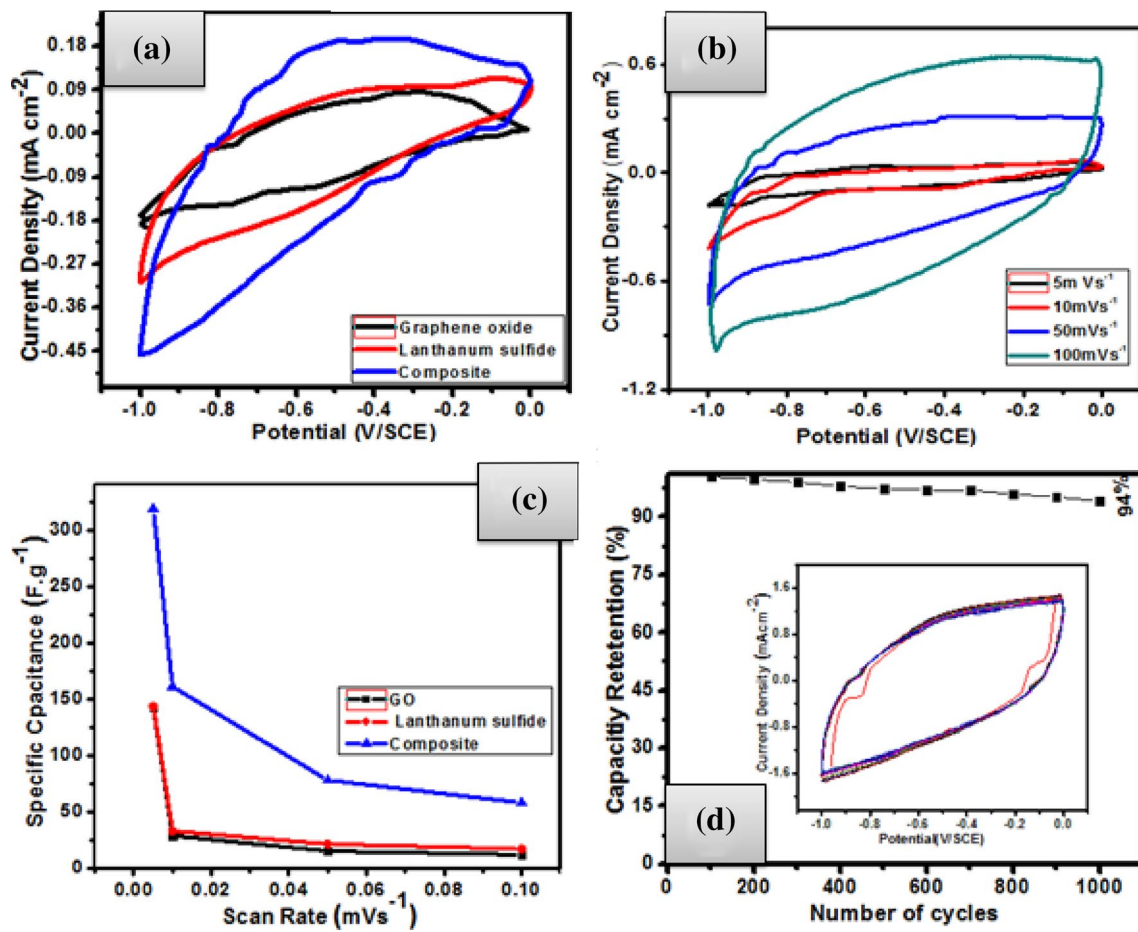
Fig. 4 **a** CV curves of GO, lanthanum sulfide and composite electrodes at 5 mV s^{-1} scan rate, **b** CV curves of composite electrode at different scan rates, **c** variation of specific capacitance Vs scan rate of GO, lanthanum sulfide, and composite electrode and **d** capacitive retention of composite electrode for 1000 CV cycles at 100 mV s^{-1} scan rate with respect to cycle numbers and inset displays CV curves of composite electrode at different cycles in 1 M Na$_2$SO$_4$ electrolyte
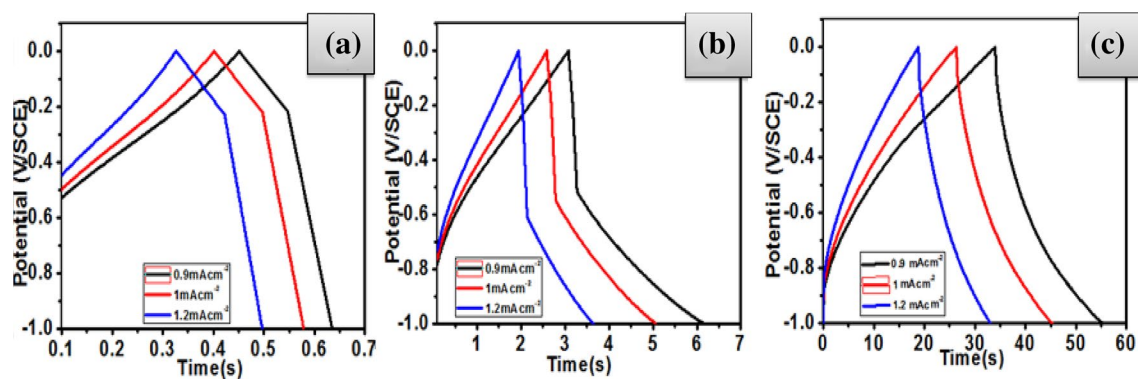

Fig. 5 Galvanostatic charge–discharge curves of **a** GO, **b** lanthanum sulfide and **c** composite electrodes at 0.9, 1 and 1.2 mA cm^{-2} current densities, respectively
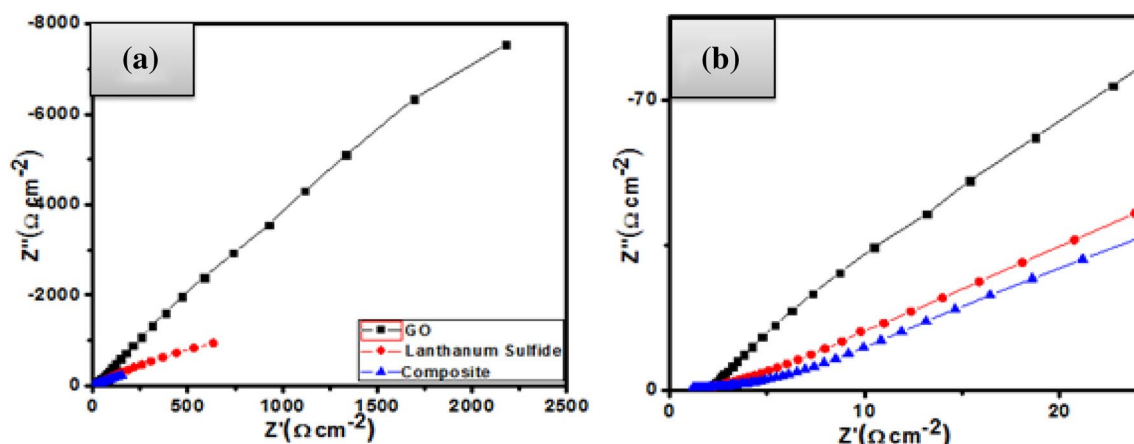
Fig. 6 **a** Nyquist plots of GO, lanthanum sulfide and composite electrodes and **b** magnified Nyquist plots of these electrodes

The galvanostatic charge/discharge curves of GO, lanthanum sulfide and composite electrodes are obtained at current densities of 0.9, 1 and 1.2 mA cm^{-2}, respectively, in the potential range − 1 to 0 V/SCE. The charge/discharge study showed the sudden potential drop in discharge curve for GO, lanthanum sulfide and composite electrodes due to the internal electrode resistance drop. All GCD curves in Fig. 5a–c show the nonlinear shapes.

Electrochemical impedance spectroscopy (EIS) technique is used for GO, lanthanum sulfide and composite electrodes studies in 1 M Na$_2$SO$_4$ electrolyte. The power output capability of supercapacitors strongly depends on the impedance of the electrode. The total impedance of the supercapacitor consists of electronic and ionic contributions. The previous is related to the intrinsic electronic resistance of the electrode particles and the interfacial resistances of particles-to-particles and particles-to-current collector. The second one is associated with the electrolyte resistance in the pores and the ionic (diffusion) resistance of ions moving in the small pores. The porosity of electrode results in the distorted semicircle in the high-frequency region and a vertically linear point in the low-frequency region. The high-frequency intercept of the semicircle on the real axis yields the solution (electrolyte) resistance (Rsol), and the diameter of the semicircle yields the charge transfer resistance (Rct) over the interface between the electrode and electrolyte.

The electrolyte for the three electrodes is totally identical. Nyquist plots in Fig. 6b of GO, lanthanum sulfide and composite electrodes in 1 M Na$_2$SO$_4$ solution in the frequency region of 100 kHz to 100 mHz at 10 mV AC amplitude show the resolved part of semi-arc. The small charge transfer and series resistances are due to the combination of lanthanum sulfide with GO sheets. GO electrode showed almost vertical line in the low-frequency region

representing the preferred capacitive behavior. A small semicircle arc is found for lanthanum sulfide and composite electrode in middle-frequency region. The series resistance (Rs: 1.1 Ω cm^{-2}) and charge transfer resistance (Rct: 2.4 Ω cm^{-2}) are estimated for composite electrode. The Nyquist clearly demonstrates that the composite electrode provides easier way (less resistance) for intercalation and deintercalation of charges compared to GO and lanthanum sulfide and also offers compact bonding with stainless steel electrode.

4 Conclusions

In this work, GO, lanthanum sulfide and lanthanum sulfide/GO composite electrodes are successfully deposited by chemical methods. The pseudocapacitive behavior of GO, lanthanum sulfide and composite electrodes is studied in 1 M Na$_2$SO$_4$ electrolyte. The composite electrode showed higher specific capacitance than GO and lanthanum sulfide due to the higher redox activity of composite electrode. The highest specific capacitance obtained for composite electrode is 312 F g^{-1} at a 5 mV s^{-1} scan rate. The EIS measurement shows that composite electrode provides low impedance compared with other two electrodes.

Compliance with ethical standards

Conflict of interest The authors declare that they have no competing interests.

References

1. Simon P, Gogotsi Y, Dunn B (2014) Where do batteries end and supercapacitor begin. Science 343:1210–1211
2. Su YS, Manthiram A (2012) Lithium–sulphur batteries with a microporous carbon paper as a bifunctional interlayer. Nat Commun 3:1166–1171
3. Xiang C, Li M, Zhi M, Manivannan A, Wu N (2013) A reduced graphene oxide/Co_3O_4 composite for supercapacitor electrode. J Power Sources 226:65–70
4. Snook GA, Kao P, Best AS (2011) Conducting-polymer-based supercapacitor devices and electrodes. J Power Sources 196:1–12
5. Singh AK, Sarkar D, Karmakar K, Mandal K, Khan GG (2016) High-performance supercapacitor electrode based on cobalt oxide–manganese dioxide–nickel oxide ternary 1-D hybrid nanotubes. ACS Appl Mater Interfaces 8:20786–20792
6. Naoi K, Naoi W, Aoyagi S (2013) New generation "nanohybrid supercapacitor". Acc Chem Res 46:1075–1083
7. Patil SJ, Kumbhar VS, Patil BH, Bulakhe RN, Lokhand CD (2014) Chemical synthesis of α-La_2S_3 thin film as an advanced electrode material for supercapacitor application. J Alloys Compd 611:191–196
8. Patil SJ, Lokhande AC, Lokhande CD (2016) Effect of aqueous electrolyte on pseudocapacitive behavior of chemically synthesized La_2S_3 electrode. J Mater Sci Semicond Process 41:132–136
9. Ghogare TT, Pujari RB, Lokhande AC, Lokhande CD (2018) Hydrothermally synthesis of nanostructured β-LaS_2 thin films. Appl Phys A Mater Sci Process 3:124–248
10. Kumata PN, Risbud SH (1993) Non-aqueous chemical synthesis of tetragonal (β-La_2S_3) lanthanum sulfide powder. Graphene and polymer composite for supercapacitor applications: a review. J Mater Sci Eng B 18:260–268
11. Yang G (2017) Graphene and polymer composite for supercapacitor applications: a review. Nano Res Lett 12:387–403
12. Stoller MD, Park S, Zhu Y, An J, Ruoff RS (2008) Graphene-based ultracapacitors. Nano Lett 8:3498–3502
13. Rakhi RB, Alshareef HN (2011) Enhancement of the energy storage properties of supercapacitors using graphene nanosheets dispersed with metal oxide-loaded carbon nanotubes. J Power Sources 196:8858–8865
14. Zhou X, Zhang J, Wu H, Yang H, Zhang J, Guo S (2011) Reducing graphene oxide via hydroxylamine: a simple and efficient route to graphene. J Phys Chem C 115:11957–11961
15. Zhu Y, Murali S, Stoller MD, Velamakanni A, Piner RD, Ruoff RS (2010) Microwave assisted exfoliation and reduction of graphite oxide for ultracapacitors. Carbon 48:2118–2122
16. Zhang K, Zhang LL, Zhao XS, Wu J (2010) Graphene/polyaniline nanofiber composites as supercapacitor electrode. ACS Chem Mater 22:3509–3516
17. Wan H, Ji X, Jiang J, Yu J, Zhang L, Bie S, Chen H, Ruan Y (2013) Hydrothermal synthesis of cobalt sulfide nanotubes: the size control and its application in supercapacitors. J Power Sources 243:396–402
18. Kumbhar VS, Jagadale AD, Gaikwad NS, Lokhande CD (2014) Modified chemical synthesis of porous α-Sm_2S_3 thin film. Mater Res Bull 56:39–44
19. Vadiyar MM, Bhise SC, Patil SK, Kolekar SS, Shelke AR, Deshpande NG, Chang JY, Ghule KS, Ghule AV (2013) Contact angle measurement: a preliminary diagnostic tool for evaluating the performance of $ZnFe_2O_4$ nano-flake based supercapacitor. J Chem Commun 00:1–3
20. Gund GS, Dubal DP, Patil BH, Shinde SS, Lokhande CD (2013) Enhance activity of chemically synthesized hybrid graphene oxide/Mn_3O_4 composite for high performance supercapacitors. Electrochim Acta 92:205–215
21. Wang A, Wang H, Zhang S, Mao C, Song J, Niu H, Jin B, Tian Y (2013) Controlled synthesis of nickel sulfide/graphene oxide nanocomposite for high-performance supercapacitor. Appl Surf Sci 282:704–708
22. Yang W, Zhao Y, He X, Chen Y, Xu J, Li S, Yang Y, Jiang Y (2015) Flexible conducting polymer/reduced graphene oxide films: synthesis, characterization, and electrochemical performance. Nanoscale Res Lett 10:222–228
23. Li X, Shen J, Li N, Ye M (2015) Fabrication of γ-MnS/rGO composite by facile one-pot solvothermal approach for supercapacitor applications. J Power Sources 282:194–201
24. Shelke AR, Lokhande AC, Pujari RB, Lokhande CD (2018) Modification in supercapacitive behavior of CoO–rGO composite thin film from exposure to ferri/ferrocyanide redox active couple. J Colloid Interface Sci 522:111–119
25. Qu B, Chen Y, Zhang M, Hu L, Lei D, Lu B, Li Q, Wang Y, Chen L, Wang T (2012) β-cobalt sulfide nanoparticles decorated graphene composite electrodes for high capacity and power supercapacitors. Nanoscale 4:7810–7816